

Expansion of the world's deserts due to global warming and vegetation-albedo feedback

Ning Zeng^{1, 2 *} and Jinho Yoon¹

¹Department of Atmospheric and Oceanic Science,
University of Maryland, College Park, USA

²Earth System Science Interdisciplinary Center and Geology,
University of Maryland, College Park, USA

* Corresponding author: Department of Atmospheric and Oceanic Science, University of Maryland, College Park, MD 20742-2425, USA; Email: zeng@atmos.umd.edu.

Many subtropical and mid-latitude regions are expected to become drier due to climate change. This will lead to reduced vegetation which may in turn amplify the initial drying due to positive feedbacks such as albedo change in response to biome redistribution, an effect rarely accounted for in climate projections. Using a coupled atmosphere-ocean-land model with a dynamic vegetation component that predicts surface albedo change, here we simulate the climate change from 1901 to 2099 with CO₂ and other forcings. In a standard IPCC-style simulation with interactive atmosphere, ocean and soil moisture, the model simulated an increase in the world's 'warm desert' area of 2.5 million km² or 10% at the end of the 21st century, mainly due to subtropical rainfall decrease and enhanced evaporative demand for soil moisture in response to greenhouse warming. In a more realistic simulation where the vegetation-albedo feedback was allowed to influence the atmospheric energy balance, the 'warm desert' area expands by 8.5 million km² or 34%. This occurs mostly as an expansion of the world's major subtropical deserts such as the Sahara, the Kalahari, the Gobi, and the Great Sandy Desert. The desiccation of these marginal zones will have major implication for the world's food supply and other ecosystem services.

A consensus has emerged in recent climate projections from the Intergovernmental Panel on Climate Change (IPCC) that rainfall in the sub-tropical regions of the world may become scarcer (1-4), driven by atmospheric circulation changes in response to greenhouse warming (5). Signs of such changes have already emerged in recent decades in regions such as the Mediterranean, southwestern US and other northern subtropical regions (6-8). However, the IPCC models have not addressed satisfactorily some of the potentially important feedbacks that could generate large changes in the climate system, such as ice sheet instability, permafrost carbon, and from land and vegetation processes. Here we address the role of one such feedback, the vegetation-albedo feedback in projected climate change.

Albedo is a leading component in vegetation-atmosphere interaction (9). Theoretical estimates suggest that an albedo increase of 0.1, typical for the conversion of forest to savanna (even larger for savanna to desert), will lead to a decrease of about 20 W m⁻² in surface absorbed solar energy. Although acting on regional scale, such a large negative radiative forcing can significantly reduce upward motion, resulting in less moisture convergence and a reduction in rainfall of approximately 1 mm d⁻¹ in a convective atmospheric environment (10). This 'Charney-mechanism' has been demonstrated to be particularly effective in semi-arid regions such as the Sahel (11-14). Vegetation feedback has also been shown to be of key importance in the drying of North Africa during the Holocene (15, 16). In cold regions, vegetation reduces albedo by masking bright snow. This may have played an important role in early Holocene boreal warming (17), and it can partially offset cooling from carbon sequestration for envisioned reforestation (18, 19). Vegetation change due to anthropogenic land-use also impacts climate during the industrial time, a factor often under-appreciated compared to fossil fuel CO₂ (20-23).

We conducted a coupled atmosphere-ocean-land-vegetation model study using the UMD Earth system model (24), a participant of the Coupled-Carbon-Cycle-Climate Model Intercomparison Project (25) (C4MIP). The land component of the model includes a physical land-surface module coupled to a dynamic vegetation model VEGAS that simulates change in vegetation functional types under climate change such as degradation of savanna to desert or replacement of tundra by forest. One important consequence of such changes is the modification of surface albedo. However, this feedback was not typically included in the C4MIP simulations even though some models had dynamic vegetation and were potentially capable of studying this effect.

To explore the role of vegetation-albedo feedback, we ‘turned on’ the vegetation albedo feedback in our model by allowing the atmospheric radiation module to ‘see’ the surface albedo A_v predicted by the vegetation model as a function of leaf area index (L):

$$A_v = A_{\min} + (A_{\max} - A_{\min}) \exp(-kL) \quad (1),$$

where $A_{\min}=0.1$ and $A_{\max}=0.45$ are the minimum and maximum albedo, respectively, and $k=0.5$ is the light extinction coefficient. This simple empirical formula is not sufficient at capturing all the possible processes responsible for the observed albedo, many of which are difficult to model mechanistically at present. To minimize potential climate drift due to full coupling, only the anomalies A'_v (changes in A_v relative to a control run) are used by the atmospheric radiation module, i.e., the changes in A_v was added onto the observed surface albedo climatology in order to capture the first-order effects due to vegetation change:

$$A = A_{\text{obs}} + A'_v \quad (2).$$

The fully coupled atmosphere-ocean-land model including dynamic vegetation and the terrestrial carbon cycle was run as in the World Climate Research Program’s Coupled Model Inter-comparison Project phase 3 (CMIP3), i.e., forced in the 20th century simulation by observed CO_2 , solar irradiance, anthropogenic and volcanic aerosol. These were fixed at the end-of-20th century values throughout the 21st century except for CO_2 which continues to rise following the IPCC A1B scenario (see Materials and Methods).

We used the criterion of LAI less than one to define desert. This is somewhat different from a common definition using precipitation, e.g., annual rainfall below 250 mm. While these two are well correlated in a stable climate regime, the vegetation based definition also captures other effects such as changes in soil moisture due to warming even if precipitation stays fixed, as demonstrated in our results below. To exclude polar and mountain deserts which are expected to shrink under warming as vegetation growth there is limited by temperature, not by rainfall, we used a criterion of observed annual mean temperature of 0°C to mask out cold regions, notably the polar regions and the Tibetan Plateau. Thus our study is on the ‘warm deserts’ inside the masked region which has a total area of 115 Mkm^2 (million km^2).

Results

Our model simulates a ‘warm desert’ area of 25 Mkm² in the early 20th century (Fig. 1), comparable to the observed 23 Mkm² using observed precipitation less than 250 mm y⁻¹ (Fig. S1). In the simulation without vegetation-albedo feedback, but including land soil-moisture feedback in addition to interactive atmosphere and ocean (thus the name AOL), the subtropical desert expands continuously from the 20th to the 21st century with substantial interannual to interdecadal variability. By the end of the 21st century the desert has increased by about 2.5 Mkm², a 10% change.

When vegetation-albedo feedback is included (AOLV), the desert area expands at a faster pace starting in the latter half of the 20th century. By 2000, the increase in desert area in the AOLV run is nearly twice as much as in the AOL run. This difference deepens further into the 21st century so that the increase in the desert area is three times more than in AOL, an 8.5 Mkm² or a 34% increase at the end of the 21st century.

We conducted an additional experiment (Obs-LV) where the land-vegetation model was run ‘offline’, driven by observed 20th century precipitation and temperature. The interannual variability in this run is somewhat larger than in the two coupled model runs which have less internal variability than Nature and are not expected to match the interannual changes event by event. Interestingly, the AOLV run with vegetation feedback also has larger interannual variability than AOL, suggesting that vegetation-albedo feedback also acts on these shorter timescales. The trend during 1951-2005 is an increase of approximately 2.5 Mkm² in both AOLV and Obs-LV, while the AOL run changed by only 1.4 Mkm² (Fig. 1). This similarity between AOLV and Obs-LV is in part fortuitous as the observed climate contains major multi-decadal variabilities such as the drought in the Sahel (26) arising from atmosphere-ocean interaction that coupled models can not reproduce on their own, especially our mixed-layer ocean model. Such agreement in model and ‘observation’ for the instrumental period suggests that the drying in the later half of the 20th century was largely caused by external forcings, not internal variability of the coupled atmosphere-ocean-land system.

The spatial pattern of the changes (Fig. 2) indicates that the regions subject to desert expansion are the Sahel, the Mediterranean region, southwest and central Asia, southern Africa and Australia. These correspond to an expansion of most ‘warm deserts’ of the world today: the Sahara, the Arabian, the Gobi, the Kalahari and the Great Sandy Desert. However, we caution that, given the coarse resolution and possible biases in our model, the exact location and extent of desert expansion may be model sensitive. For instance, we also noticed transition to desert in western US in the AOL run (not shown), but it is not seen in the AOLV run in Fig. 2. Higher-resolution models will be needed for better assessment. Nonetheless, these regions coincide broadly with the regions known to be sensitive to land-surface processes (27), lending qualitative confidence to our model results.

We also conducted experiments in which projected precipitation and temperature from 15 IPCC models were used to drive VEGAS. The projected changes in desert area, similarly

defined as LAI less than one, show that the desert area indeed increases (Fig. S2). These IPCC models all include interactive land-surface model that dynamically predicts soil moisture and its feedback through evapotranspiration, and is similar to our AOL run. The IPCC model average predicts somewhat smaller desert expansion in the decades around year 2000 compared to our AOL run, but quickly catches up in the 21st century and have slightly larger increase (over 3 Mkm² more desert) by the end of the 21st century. Although all the IPCC models exhibit an expansion of deserts, there are large differences in magnitude, ranging from negligible change in some models to 7-9 Mkm² increase in some other models, approaching the prediction of our AOLV simulation.

The magnitude of desert expansion predicted by our model and the IPCC models is striking, especially the 34% increase in the AOLV run with vegetation-albedo feedback. Our analysis suggests that this is the result of a chain of processes and feedbacks initiated by greenhouse warming. We identify the key steps as following.

(1) Changes in the tropical atmospheric circulation in response to greenhouse warming lead to a broadening of the subsidence branch of the Hadley circulation which further suppresses rainfall in the subtropics that is already dry (meteorological drought). This contrasts increased rainfall in the Inter-tropical Convergence Zone and the high latitude regions (2, 5).

(2) These dry regions further invade into adjacent area as measured by soil moisture (hydrological drought) because global warming increases evaporative demand even if rainfall does not change, thus leading to less soil moisture. Indeed, using precipitation, instead of soil moisture or LAI as criterion, both the AOL run and the IPCC model mean exhibit little net change in desert area (1) (not shown). Thus a region with minor increase in rainfall can be outcompeted by increased evaporation loss, resulting in decreased soil moisture. Because vegetation does not use rainfall directly, soil moisture is a better measure than precipitation for ecosystem impact.

(3) The area with reduced vegetation further expands from the area with decreased soil moisture because of heat stress and respiration loss at higher temperature.

These successive effects are summarized in Fig. 3 where 41 Mkm² land (36% of the 'warm' region) has reduced precipitation, but 57 Mkm² (50%) has less soil moisture, and 60 Mkm² (52%) has less vegetation as measured by LAI. Spatially, this expansion of 'drought' corresponds to widespread drying in Africa, the Mediterranean, Asia, and to lesser degree North America and Australia (Fig. S3).

(4) A major reduction in vegetation in these regions leads to increased surface albedo, which reduces heat input and moist static energy. Consequently the subsidence typical of these subtropical regions intensify, leading to reduced moisture convergence and precipitation (11). Such mechanism is particularly effective in the thermally driven convective region which includes tropics and warm-season mid-latitude regions (10). This additional reduction in precipitation is further amplified by the three processes discussed above. The final effect of vegetation-albedo feedback is an additional 9 Mkm²

or 8% of the ‘warm’ land area having reduced precipitation. This chain of feedbacks is illustrated in Fig.3.

The above analysis has focused on changes in the size of the area satisfying a preset threshold in LAI, precipitation or soil moisture. An alternative perspective that is particularly illuminating for understanding the feedback is the strength of change in a given region. We selected the marginal zones that are not desert in the 20th century, but become desert (LAI changes from above 1 to below 1) in the 21st century from the AOLV run (colored regions in Fig. 2). As shown in Fig. 4, the average rainfall in these regions decreased from 1.3 mm d⁻¹ at 1901 to about 0.1 mm d⁻¹ at the end of the 21st century, and soil wetness from 28% to 5%, LAI from 2.6 to 0.3, thus near-complete desiccation. The average albedo increases from 0.26 to 0.44, thus contributes to a large vegetation-rainfall feedback. In contrast, in the absence of vegetation-albedo feedback (AOL), the changes are substantially smaller (not shown). The mechanism of such positive feedback has been highlighted and quantified in analytical models (10, 11) and supported by global climate models (13, 28, 29). In addition, the model also shows a loss in vegetation and soil organic carbon that begins in the late 20th century and reaches 16 GtC (gigatonne or 10¹² kg carbon) at the end of the 21st century. Further analysis shows that it is mostly due to the loss of vegetation biomass.

Conclusion

The IPCC models have traditionally focused on one aspect of anthropogenic impact on the climate system, namely, warming due to increase in atmospheric greenhouse gases. Although a sensible approach initially, it misses many other important direct or feedback effects. Our modeling results suggest that one such process, vegetation-albedo feedback may accelerate the expansion of the world’s major subtropical deserts under global warming, thus adding pressure to these marginal zones that are already vulnerable to natural and human-induced changes.

Materials and Methods

The description of our model and the IPCC models are in the Supporting Information and reference (24). Briefly, the physical climate components of our model consist of a global version of the atmospheric model QTCM, the physical land-surface model SLand, and a slab mixed layer ocean model with Q-flux to represent the effects of ocean dynamics. The dynamic vegetation and carbon model VEGAS is coupled to SLand, mainly through soil moisture and photosynthesis control on evapotranspiration. A key aspect of relevance here is the prediction of surface albedo that depends on LAI and influences the atmospheric energy budget. The coupled atmosphere-ocean-land-vegetation model was spun up to steady state with repetitive 1870 forcings and then run to 2099. The model was forced from 1870 to 2000 by observed CO₂, variabilities in solar irradiance (to 2000), direct anthropogenic (to 1990) and volcanic aerosol forcings (to 1999), and set to constant afterwards, and by a CO₂ scenario A1B after 2000. Thus, this is not the C4MIP-style full carbon-climate coupling as in ref. (24), but rather the IPCC CMIP3-style

simulation, except of course we also included vegetation-albedo feedback in our AOLV run, typically not represented in the IPCC models. All model components were run at a resolution of $5.625^{\circ} \times 3.75^{\circ}$, a limitation set by the atmospheric model. The atmospheric component was run at 20 minute time step while all other components were run once a day.

Acknowledgements. We thank the CMIP3 modeling groups for providing their model output through PCMDI model archive, E. Kalnay for stimulating discussions and support from NSF-ATM0739677, NOAA-NA04OAR4310114, and NOAA-NA17EC1483.

References

1. Burke EJ, Brown SJ, & Christidis N (2006) *J. Hydrometeorol.* **7**, 1113-1125.
2. Meehl GA, Stocker TF, Collins WD, Friedlingstein P, Gaye AT, Gregory JM, Kitoh A, Knutti R, Murphy JM, Noda A, *et al.* (2007) in *Climate Change 2007: The Physical Science Basis. Contribution of Working Group I to the Fourth Assessment Report of the Intergovernmental Panel on Climate Change*, eds. Solomon S & D. Qin MM, Z. Chen, M. Marquis, K.B. Averyt, M. Tignor and H.L. Miller (Cambridge University Press, Cambridge, UK).
3. Neelin JD, Munnich M, Su H, Meyerson JE, & Holloway CE (2006) *Proc. Natl. Acad. Sci. U. S. A.* **103**, 6110-6115.
4. Sheffield J & Wood EF (2008) *Clim. Dyn.* **31**, 79-105.
5. Held IM & Soden BJ (2006) *Journal of Climate* **19**, 5686-5699.
6. Mariotti A, Zeng N, Yoon J, Artale V, Navarra A, Alpert P, & Li L (2008) *Environ. Res. Lett.* **3**, 044001.
7. Zhang XB, Zwiers FW, Hegerl GC, Lambert FH, Gillett NP, Solomon S, Stott PA, & Nozawa T (2007) *Nature* **448**, 461-U464.
8. Seager R, Ting MF, Held I, Kushnir Y, Lu J, Vecchi G, Huang HP, Harnik N, Leetmaa A, Lau NC, *et al.* (2007) *Science* **316**, 1181-1184.
9. Bonan GB (2008) *Science* **320**, 1444-1449.
10. Zeng N & Neelin JD (1999) *Journal of Climate* **12**, 857-872.
11. Charney JG (1975) *Quarterly Journal of the Royal Meteorological Society* **101**, 193-202.
12. Dirmeyer PA & Shukla J (1996) *Quarterly Journal of the Royal Meteorological Society* **122**, 451-482.

13. Zeng N, Neelin JD, Lau KM, & Tucker CJ (1999) *Science* **286**, 1537-1540.
14. Xue YK & Shukla J (1993) *Journal of Climate* **6**, 2232-2245.
15. deMenocal P, Ortiz J, Guilderson T, Adkins J, Sarnthein M, Baker L, & Yarusinsky M (2000) *Quaternary Sci. Rev.* **19**, 347-361.
16. Claussen M, Kubatzki C, Brovkin V, Ganopolski A, Hoelzmann P, & Pachur HJ (1999) *Geophysical Research Letters* **26**, 2037-2040.
17. Foley JA, Kutzbach JE, Coe MT, & Levis S (1994) *Nature* **371**, 52-54.
18. Betts RA (2000) *Nature* **408**, 187-190.
19. Jackson RB, Randerson JT, Canadell JG, Anderson RG, Avissar R, Baldocchi DD, Bonan GB, Caldeira K, Diffenbaugh NS, Field CB, *et al.* (2008) *Environ. Res. Lett.* **3**, 5.
20. Hansen JE, Sato M, Lacis A, Ruedy R, Tegen I, & Matthews E (1998) *Proc. Natl. Acad. Sci. U. S. A.* **95**, 12753-12758.
21. Kalnay E & Cai M (2003) *Nature* **423**, 528-531.
22. Pielke RA (2005) *Science* **310**, 1625-1626.
23. Cook BI, Miller RL, & Seager R (2008) *Geophysical Research Letters* **35**.
24. Zeng N, Qian HF, Munoz E, & Iacono R (2004) *Geophysical Research Letters* **31**.
25. Friedlingstein P, Cox P, Betts R, Bopp L, Von Bloh W, Brovkin V, Cadule P, Doney S, Eby M, Fung I, *et al.* (2006) *Journal of Climate* **19**, 3337-3353.
26. Folland CK, Palmer TN, & Parker DE (1986) *Nature* **320**, 602-607.
27. Koster RD, Dirmeyer PA, Guo ZC, Bonan G, Chan E, Cox P, Gordon CT, Kanae S, Kowalczyk E, Lawrence D, *et al.* (2004) *Science* **305**, 1138-1140.
28. Wang G, Eltahir EAB, Foley JA, Pollard D, & Levis S (2004) *Clim. Dyn.* **22**, 625-637.
29. Crucifix M, Betts RA, & Cox PM (2005) *Clim. Dyn.* **24**, 457-467.

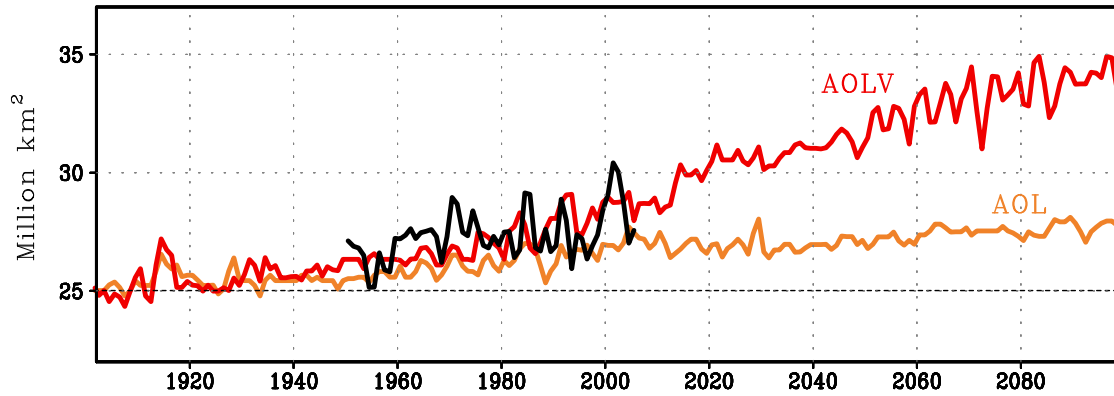


Figure 1. Area of the world's 'warm deserts' in million km² from 1901 to 2099 as simulated by the fully coupled atmosphere-ocean-land-vegetation model in response to greenhouse gas and other forcings. Desert is defined as leaf area index (LAI) less than 1. The difference between the AOLV run (red line) and the AOL run (brown) is that AOLV has vegetation-albedo feedback, which leads to much larger expansion in the desert area. Also plotted is the land-vegetation model forced by observed climate (Obs-LV; black) for 1951-2005, and its result has a vertical offset to match the AOLV run in the 1950s.

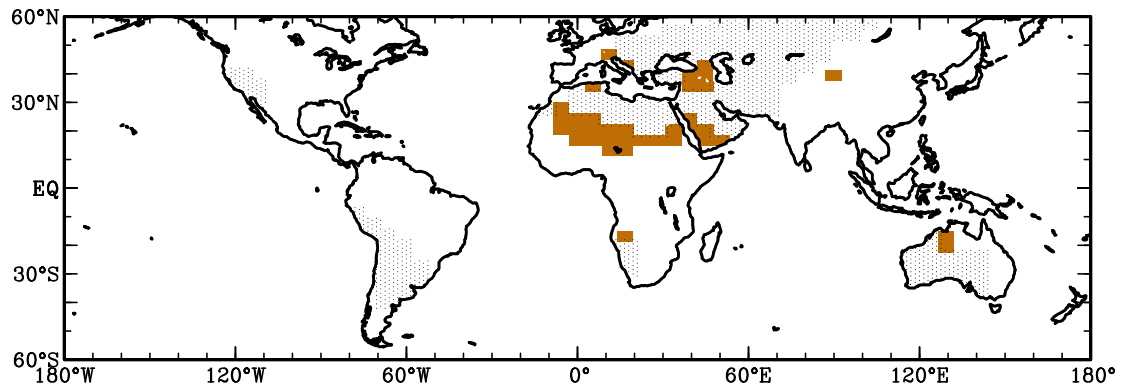


Figure 2. Marginal land projected to change from non-desert in the 20th century to desert in the 21st century in the AOLV run with albedo feedback, shown in brown color as the difference between the average of 2070-2099 and that of 1961-1990. Stippled region is model's 20th century desert area (LAI less than 1 during 1961-1990).

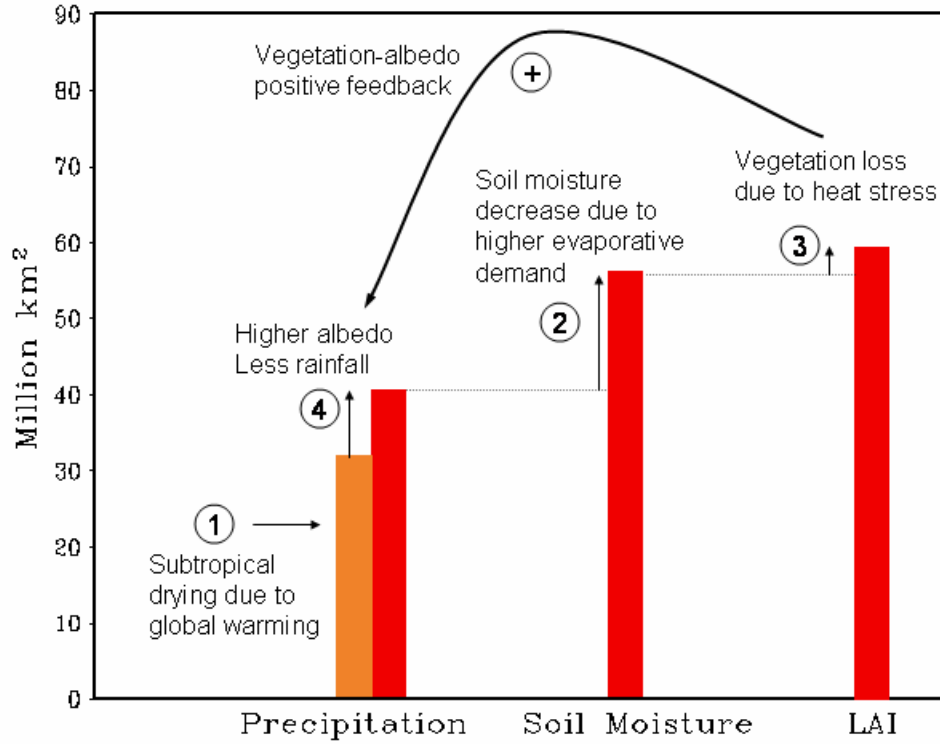


Figure 3. The size of the area where precipitation, soil moisture, or LAI decreases from the 20th to the 21st century for the AOLV run (red bars), and the size of the area with decreasing precipitation for the AOL run (brown bar). More land area sees reduction in soil moisture compared to precipitation, and even more area has vegetation loss. Approximately 9 million km² more land area has decreasing precipitation in AOLV than in AOL due to a positive vegetation-albedo feedback. The numbered processes correspond to the description in the text.

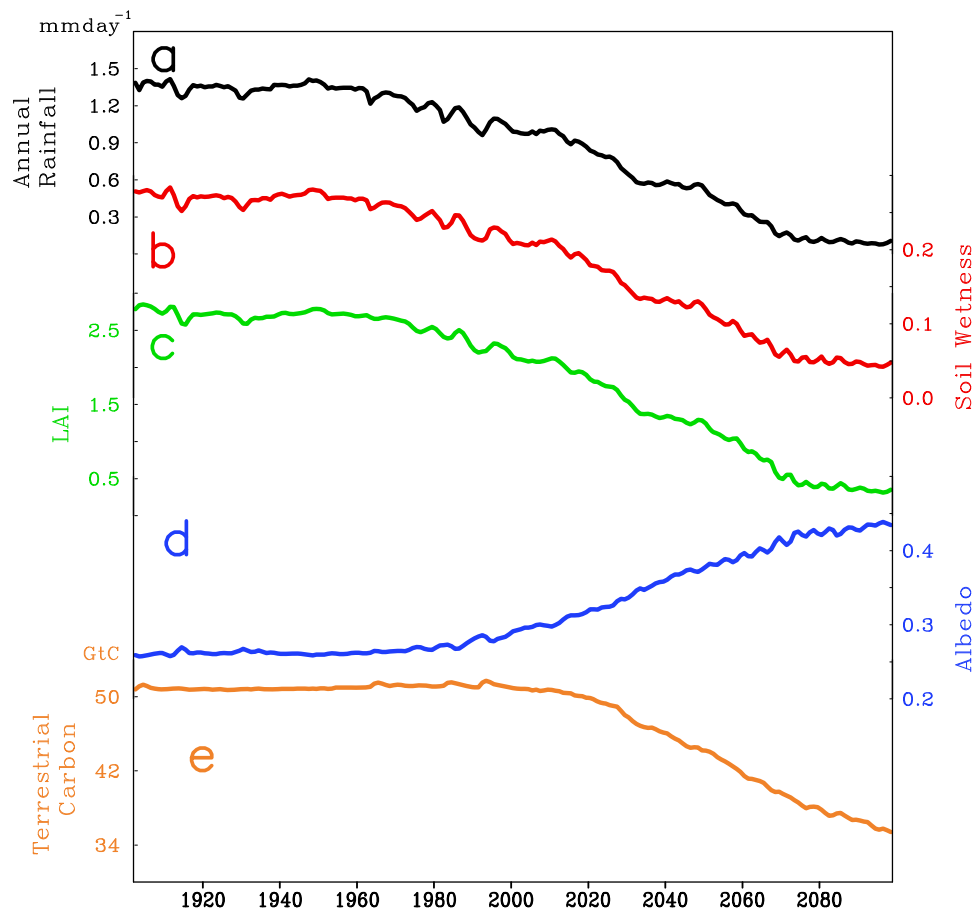


Figure 4. Time evolution of (a) annual precipitation, (b) soil wetness, (c) LAI, (d) surface albedo and (e) total land carbon, for the marginal land area that changes from non-desert to desert (colored area in Fig. 2).

Supporting Information

1. IPCC models and VEGAS

The IPCC models are multi-model ensembles, run with radiative forcings estimated for the twentieth century and the SRES A1B scenario for twenty-first century change. The models included are listed in the table below. Details of the model can be found at http://www-pcmdi.llnl.gov/ipcc/model_documentation/ipcc_model_documentation.php.

Model Name	Institution	Country
CSIRO-MK3	Commonwealth Scientific and Industrial Research Organization	Australia
ECHAM5	Max Planck Institute	Germany
GFDL-CM2.0	NOAA/Geophysical Fluid Dynamics Laboratory	USA
GFDL-CM2.1	NOAA/Geophysical Fluid Dynamics Laboratory	USA
HadCM3	UKMO/Hadley Centre	UK
HadGEM1	UKMO/Hadley Centre	UK
GISS-EH	NASA/Goddard Institute for Space Studies	USA
GISS-ER	NASA/Goddard Institute for Space Studies	USA
INGV	Instituto Nazionale di Geofisica e Vulcanologia	France
IPSL-CM4	Institut Pierre Simon Laplace	France
MIROC-3.2-medres	Center for Climate System Research, University of Tokyo	Japan
MIROC-3.2-hires	Center for Climate System Research, University of Tokyo	Japan

MRI-CGCM2	Meteorological Research Institute	Japan
NCAR-CCSM3	National Center for Atmospheric Research	USA
NCAR-PCM1	National Center for Atmospheric Research	USA

Model variables from these 15 models were interpolated onto a common $2.5^{\circ} \times 2.5^{\circ}$ grid. The change from late 21st century (2070-2099 average) relative to a base period climatology (1961-1990 average) was computed for all 15 models. The offline VEGAS model was forced individually by the 15 IPCC model climates for variables such as precipitation and temperature for 1901-2099, and then the results are analyzed for their changes (Fig. S2)

The terrestrial carbon model Vegetation-Global-Atmosphere-Soil (1-3) (VEGAS) simulates the dynamics of vegetation growth and competition among different plant functional types (PFTs). It includes 4 PFTs: broadleaf tree, needleleaf tree, cold grass, and warm grass. The different photosynthetic pathways are distinguished for C3 (the first three PFTs above) and C4 (warm grass) plants. Phenology is simulated dynamically as the balance between growth and respiration/turnover. Competition among PFTs is determined by climatic constraints and resource allocation strategy such as temperature tolerance and height dependent shading. Unlike many other global dynamic vegetation models, whether a PFT is deciduous or evergreen is not prescribed, but rather dynamically determined. The relative competitive advantage then determines fractional coverage of each PFT with possibility of coexistence. Accompanying the vegetation dynamics is the full terrestrial carbon cycle, starting from photosynthetic carbon assimilation in the leaves and the allocation of this carbon into three vegetation carbon pools: leaf, root, and wood. After accounting for respiration, the biomass turnover from these three vegetation carbon pools cascades into a fast soil carbon pool, an intermediate and finally a slow soil pool. Temperature and moisture dependent decomposition of these carbon pools returns carbon back into the atmosphere, thus closing the terrestrial carbon cycle. A fire module includes the effects of moisture availability, fuel loading, and PFT dependent resistance and captures fire contribution to interannual CO₂ variability (4, 5). The vegetation component is coupled to land and atmosphere through a soil moisture dependence of photosynthesis and evapotranspiration, as well as dependence on temperature, radiation, and atmospheric CO₂. Unique features of VEGAS include a vegetation height dependent maximum canopy which introduces a decadal time scale that can be important for feedback into climate variability; a decreasing temperature dependence of respiration from fast to slow soil pools (6); and a balanced complexity between vegetation and soil processes. VEGAS has also been validated on interannual timescales in the tropics (3, 4), and for temperate and boreal regions as a participant of the ongoing North American Carbon Program model-data intercomparison. The other

components of the UMD Earth system model are described and referenced in the reference (2).

2. Figures S1-S3

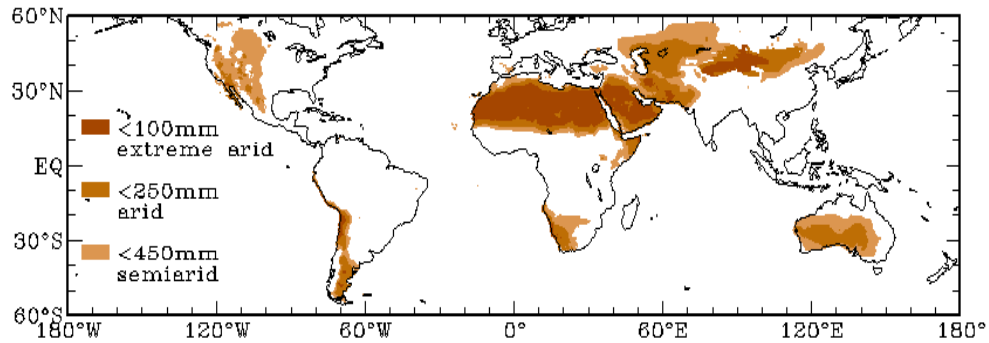


Figure S1. The world distribution of “warm deserts” with differing degree of aridity: extremely-arid, arid and semi-arid defined using observed precipitation ($0.5^\circ \times 0.5^\circ$ resolution) less than 100, 250, 450 mm/y, respectively (upper panel). The ‘warm’ regions are defined as the area with annual mean observed surface air temperature greater than 0°C which excludes notably the Polar regions and the Tibetan Plateau. The coarse resolution of the model ($5.625^\circ \times 3.75^\circ$) (Fig. 2) is not able to identify many mountainous regions such as the Andes.

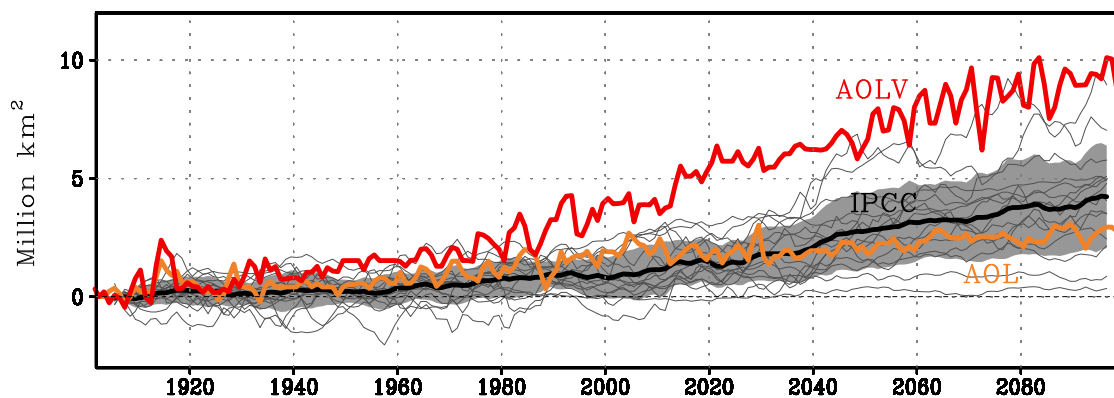


Figure S2. The expansion of deserts as in Fig. 1, but also plotted are the results from VEGAS driven by the precipitation and temperature projected by 15 IPCC models. Thick black line is the average while the individual IPCC-VEGAS model results are shown as gray lines and the shading is their standard deviation.

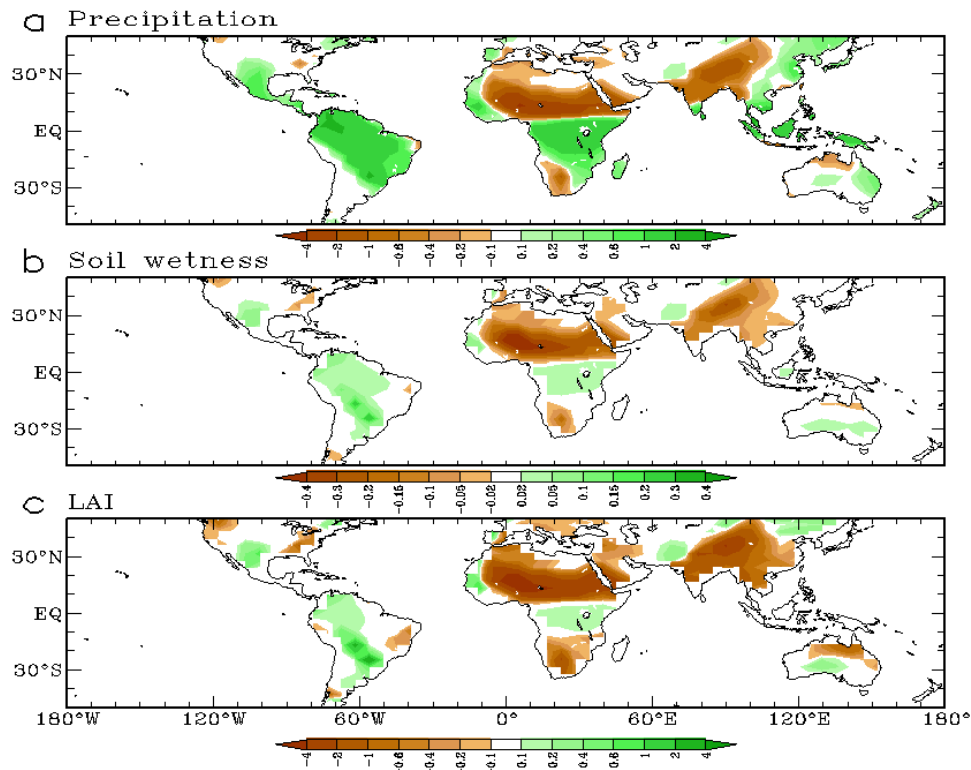


Figure S3. The difference between the averages of 2070-2099 and 1961-1990 for the AOLV run, showing successively more regions with decreasing precipitation (mm d^{-1}), soil wetness (fraction), and LAI (m^2/m^2). Figure 3 is a summary of these spatial changes.

References

1. Zeng N (2003) *Advances in Atmospheric Sciences* **20**, 677-693.
2. Zeng N, Qian HF, Munoz E, & Iacono R (2004) *Geophysical Research Letters* **31**.
3. Zeng N, Mariotti A, & Wetzel P (2005) *Global Biogeochemical Cycles* **19**.
4. Zeng N, Qian HF, Roedenbeck C, & Heimann M (2005) *Geophysical Research Letters* **32**.
5. Qian H, Joseph R, & Zeng N (2008) *Tellus Series B-Chemical and Physical Meteorology* **60**, 537-550.
6. Liski J, Ilvesniemi H, Makela A, & Westman CJ (1999) *Ambio* **28**, 171-174.